The symmetric-asymmetric transition of the sponge phase : I. Effect of the salinity

C. Vinches, C. Coulon, D. Roux

Classification
Physics Abstracts
64.70 — 77.40 — 78.35

The symmetric-asymmetric transition of the sponge phase : I. Effect of the salinity

C. Vinches, C. Coulon and D. Roux

Centre de Recherche P. Pascal, CNRS, Avenue du Dr Schweitzer, 33600 Pessac, France

(*Received 7 January 1994, received in final form 23 March 1994, accepted 28 March 1994*)

Résumé. — Nous présentons une étude systématique de systèmes pseudoternaires : eau salée, pentanol, SDS pour des concentrations en sel variant de 20 à 80 g/l de NaCl. Dans la zone diluée du diagramme de phase, le système à plus faible salinité est connu pour présenter une transition de phase continue entre une phase de membranes interconnectées aléatoirement, la phase éponge (symétrique) et une phase asymétrique. Nous trouvons la même topologie du diagramme de phase lorsque l'on augmente la concentration en sel et nous étudions l'évolution des caractéristiques de la transition symétrique/asymétrique. Dans une première partie des expériences de diffusion de la lumière sont décrites. Nous montrons que l'intensité diffusée doit être analysée en terme de produit d'un facteur de structure et d'un facteur de forme. La contribution du facteur de forme permet d'obtenir directement la taille géométrique de la phase (la distance moyenne entre les membranes) sans que l'on utilise un modèle thermodynamique et permet cependant d'obtenir sans ambiguïté la position de la transition symétrique/asymétrique. Le facteur de structure renseigne sur le comportement critique à la transition. La dépendance en fréquence de la conductivité électrique (dans le domaine 100 Hz-15 MHz) a également été mesurée pour la première fois dans ce type de systèmes. Ces phases peuvent être considérées comme un composite constitué d'un solvant conducteur et d'une membrane diélectrique et les données sont analysées en terme de conductivité basse fréquence (DC) conduisant à un facteur « d'obstruction » et une constante diélectrique fortement dépendante de la fréquence. Loin de la transition de phase S/A, le facteur d'obstruction est constant et la constante diélectrique montre une relaxation de Debye. Des lois d'échelle simples sont obtenues pour les variations de l'intensité et de la fréquence en fonction de la dilution. Ceci indique que le mode est relié à la « structure locale » de la phase éponge. Au voisinage de la transition de phase S/A, une autre relaxation, qui se superpose au mode précédent, est observée à des fréquences plus basses. En parallèle, un écart aux lois d'échelles du mode de Debye et un accroissement du facteur d'obstruction peut être interprété comme une preuve de l'existence de défauts (des trous ?) sur la membrane. Nous montrons que l'importance de ces défauts augmente lorsque la concentration en sel diminue.

Abstract. — A systematic study of pseudoternary systems made of salted water, pentanol and SDS is presented for salt concentrations ranging from 20 to 80 g/l of NaCl. In the dilute part of the phase diagram, the system with the lowest salt concentration is known to present a continuous phase transition between phases of randomly interconnected membranes, namely a sponge (symmetric) and an asymmetric phase. The same topology is found as the salt concentration is increased and the evolution of the characteristics of the symmetric-asymmetric phase transition is studied. Light

scattering experiments are first described. We show that the scattered intensity should be analysed in terms of a product of a structure and a form factor. The latter contribution gives directly the geometrical size of the phase (the mean distance between the membranes) without using any thermodynamical model and therefore gives an unambiguous location of the symmetric-asymmetric phase transition. The structure factor gives the critical behaviour at the phase transition. Electrical conductivity as a function of the frequency (in the range 100 Hz-15 MHz) has also been measured for the first time in this kind of systems. These phases can be considered as composites of a conducting solvent and a dielectric membrane and the data are analysed in terms of a low frequency (DC) conductivity leading to an « obstruction » factor and a dielectric constant strongly dependent on the frequency. Far from the S/A phase transition, the obstruction factor is constant and the dielectric constant shows a single Debye-like relaxation. Simple scaling laws are found for the variation of the intensity and of the frequency as a function of dilution. This indicates that the mode probes the « local structure » of the sponge phase. Near the S/A phase transition, in addition to this mode, another dielectric relaxation is observed at lower frequencies. At the same time, a departure from the scaling laws of the Debye mode and an increase of the obstruction factor can be interpreted as evidence for defects (holes ?) on the membrane. We show that the role of these defects increases as the salt concentration decreases.

1. Introduction.

Surfactants in solution are well-known to form a wide variety of phases, even in the dilute region of the phase diagram. In particular, a phase of randomly connected membranes separating two identical volumes of solvent, the so-called sponge (or L3) phase has been recently discovered [1] and independently proposed theoretically [2]. The structure of the sponge phase can be described as a random surface made of the membrane separating a volume into two identical but not connected sub-volumes of solvent (arbitrarily labelled In and Out). One can easily generate the description of such a phase by taking an Ising model in the paramagnetic state and locating the membrane at the interface between the up and down domains, assuming that both domains correspond to the solvent. Since there is no difference between the sub-volumes up and down the free energy of the phase has to be symmetric upon a change of definition of what is up and down. This symmetry can be equivalently described by the fact that the two sub-volumes defined by the membrane surface are equivalent in volumes or by the average curvature of the membrane which is zero. Because of its unique symmetry, the sponge is also labelled as the symmetric (S) phase. It is now well established that the sponge phase can be found in various systems incorporating either ionic or non-ionic surfactants [3, 4]. Because of its peculiar topology, the sponge phase exhibits very striking properties. Many of them can be deduced in terms of scaling laws [5]. Indeed, when adding solvent to a sponge phase, neglecting logarithmic corrections due to fluctuations [6], the topology remains the same. The only modification is an increase of the mean distance ξ_0 between the membranes which is proportional to the inverse of the membrane volume fraction ϕ. Because both the entropy and the elastic energy are not size dependent, the free energy of a sponge is easily calculated to be of the order of $k_B T$ per basic cell of size ξ_0. Consequently the free energy density scales as $1/\xi_0^3$, i.e., is proportional to ϕ^3. This simple scaling of the free energy per unit volume indicates that all thermodynamical properties will simply scale with the basic size of the sponge and consequently with the volume fraction ϕ. For example the light scattering intensity extrapolated at $q = 0$ should vary mainly like $1/\phi$. These scaling laws are in fact observed experimentally and confirm the distinctive symmetry of the sponge phase.

Another important question is the problem of the stability of the sponge phase. The symmetry described above can be broken thus leading to an asymmetric phase where the two sub-volumes will now be different and the average curvature of the membrane different from zero. Keeping the analogy to an Ising model, this phase would correspond to a ferromagnetic phase. Ultimately the asymmetric phase corresponds to a phase of vesicles. The fact that the passage from the sponge phase to the vesicle phase corresponds to a breaking of symmetry indicates that a phase transition between these two phases is always expected. Due to the coupling between the S/A order parameter and the membrane volume fraction, this Symmetric/Asymmetric (S/A) phase transition can be either first order or second order. When it is second order, the peculiar symmetry of the sponge is spontaneously broken to give an asymmetric (A) phase where the two domains of solvent separated by the membrane are no longer equivalent. The A phase has the same symmetry as a micellar (L1) phase and the A phase is expected to evolve continuously into a standard L1 phase composed of vesicles, micelles or eventually isolated surfactant molecules without any phase transition. The continuous S/A phase transition predicted theoretically [2, 6] has been recently experimentally observed in a pseudo-ternary system of salted water (with 20 g/l of NaCl), pentanol and sodium dodecyl sulfate [7].

The description of the sponge in terms of two interconnected volumes of solvent and the simple scenario for the S/A phase transition implies that no defects are present in the membrane. In other words, the energy per unit length which is necessary to generate free edges or seams is assumed (unrealistically) to be infinite. Within this limit, the S/A phase transition can be described as the condensation of an Ising-like order parameter η, coupled to the membrane density. In a real system, we expect the existence of a finite density of defects which are activated by thermal fluctuations. A recent theoretical study based on an analogy with Gauge-Higgs systems shows that the symmetry of the sponge survives to a finite density of defects as long as the defect energy (normalized to $k_B T$) is above a critical value [8]. When this condition is not satisfied, a new phase can be present, the sponge with free edges (SFE) where infinite lines of defects are present. This phase is in fact asymmetric in nature but may be distinctively separated from a classical asymmetric phase by the fact that a phase transition between the SFE and the Asymmetric phase may be observed. Consequently, there exist two scenarii for a symmetric sponge phase to disappear, one is the classical Symmetric/Asymmetric scenario where the integrity of the membrane is not affected by the transition and the second one corresponds to a proliferation of edges destroying the very nature of the membrane. Taking into account that no clear order parameters can be defined in the second case, it is probably a very difficult task to connect experiments and theories. However, it is certainly relevant to discuss the role played by the defects in the second order phase transitions observed experimentally. As we show in the following, this question may be addressed through the detailed study of the role of the salt concentration in the ternary systems mentioned previously. In this paper (paper I), we compare the properties of systems with salt concentrations of 20 g/l and upper concentrations. In these cases, the same topology of the phase diagram is found, with a single line of second order phase transitions. We show that the simple scheme for a S/A phase transition previously described is correct, although defects are present in the sponge phase near the transition line. In a following paper [9], labelled II, a system with a lower salt concentration (6.5 g/l) will be studied where the role of the defects is even more important. In this case, a more complex topology of the phase diagram is eventually found to be related to the presence of a sponge with free edges.

We have studied in detail the salinity 20 g/l and we will present first the data for this salinity. This system has been previously studied and the results of light scattering allowed us to demonstrate that a continuous S/A transition takes place [7]. However, we have detailed much

more the approach of the phase transition using light scattering and impedance measurements. We have re-analysed the light scattering data and we show that, in this new approach, owing to the extreme dilution of the phase, we have to take into account the form factor of the membrane in order to correctly account for the experimental data. The basic conclusion of the first analysis is not qualitatively changed and we show that an unambigous location of the S/A phase transition is readily obtained from this new analysis. Moreover, this work is completed with impedance measurements. The analysis of the dielectric properties as a function of the frequency exhibit, in addition to the low frequency conductivity discussed in terms of obstruction factor, a high frequency (Debye-like) mode whose amplitude and characteristic frequency seem to be directly related to the sponge cell size. In addition, very close to the transition, another dielectric relaxation appears at lower frequency that may be related to critical fluctuations. The complete analysis and a careful comparison between the light scattering data and the impedance measurements show that defects appear when the S/A transition is approached. However, these defects do not seem to affect the S/A transition qualitatively. In a second part, the effect of increasing the salt concentration is examined (30, 40, 50 and 80 g/l) and a comparison of these results with those obtained for 20 g/l is done. The increase of the salinity seems to decrease the number of defects at the S/A transition and large salinity seems to correspond to a classical S/A transition where the effect of defects can be considered as marginal. All the experimental work described in this paper was made at the same temperature, $T = 22$ °C.

2. Study of the system at 20 g/l of NaCl.

A previous study of this system, which has already been published, shown the existence of a domain where a sponge phase is stable and the occurrence of a line of maxima of turbidity, i.e., a line where both the turbidity (defined as the ratio between the incident and transmitted intensity) and the scattered intensity at a wave vector extrapolated to zero are maximum [7, 10]. From light scattering, this line has been identified to be a line of second order S/A phase transitions. The phase diagram is given in figure 1a. Note the existence of a critical point which is approximately located at the end of the transition line. The dashed line is the dilution line along which samples described in the following were prepared. Compared to the previous study, more experimental points have been prepared specially close to the S/A transition. In the next two sections, we first briefly review light scattering results in order to propose a new way of analysing the data. In order to justify this analysis, let us first consider what can be expected in general from the scattering of a sponge phase whatever the scattering technique used.

2.1 SCATTERING OF A SPONGE PHASE. — Figure 2 shows a characteristic curve of the intensity I as a function of the wave vector q of a sponge phase (in the symmetric state). We have presented this curve with two different plots in order to exhibit clearly the different regimes of scattering. A sponge phase can be described by three different length scales that we will use to describe the different scattering regimes. The smallest length is a molecular one corresponding to the thickness of the membrane (δ). The second length is ξ_0 the cell size and characterizes the typical length for which the membrane can be considered as flat, it is also the membrane-membrane characteristic distance. Above the cell size, the scattering will be dominated by the membrane density-density correlation function which is largely influenced by the In/Out fluctuations, the characteristic length of these fluctuations being labelled ξ_η. For q vector larger than $2\ \pi/\delta$ the scattering is dominated by the interface between the hydrophobic part of the membrane and the water, it varies as $1/q^4$, this is known as the Porod law. Taking into account the typical value for δ (20/30 Å) this range of scattering can only be observed with either neutron scattering or X-ray. For q vector between $2\ \pi/\delta$ and $2\ \pi/\xi_0$ the scattering is

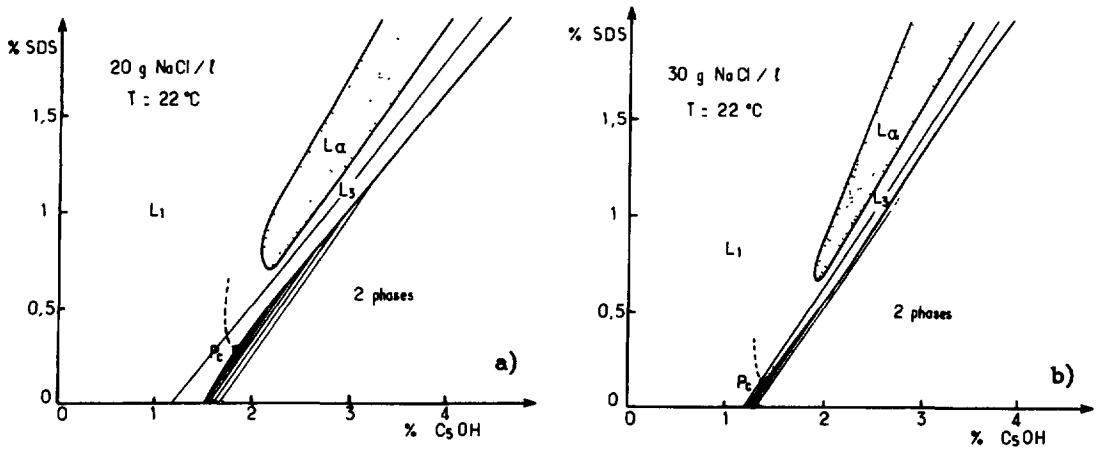

Fig. 1. — Phase diagram of two of the studied systems. (a) 20 g/l, (b) 30 g/l. The sponge (L3), lamellar (Lα) and micellar (L1) domains and the two-phase region are located. The transition line (dashed) and the dilution line (continuous line) along which the samples were prepared are also given. Note also the position of the critical point (P_C).

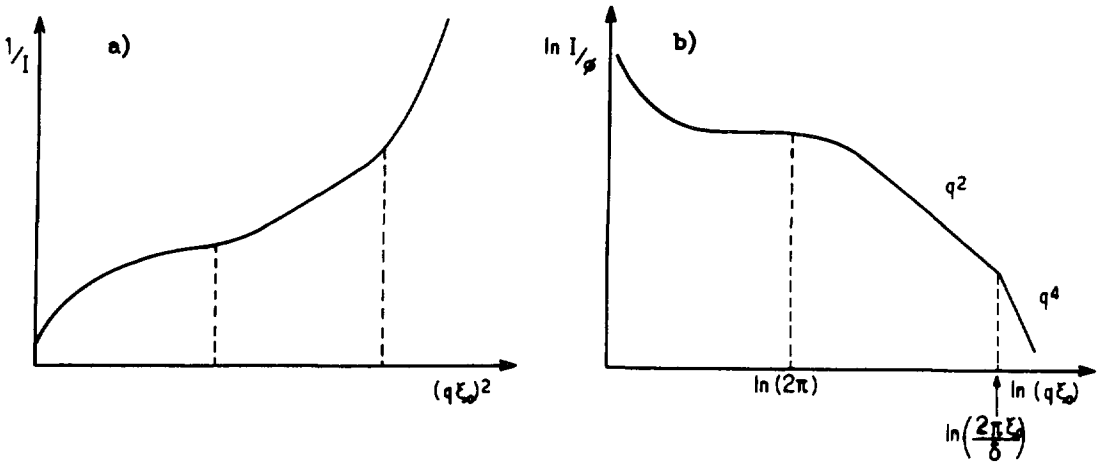

Fig. 2. — Theoretical light scattering intensity expected for the sponge phase. (a) Linear plot of the inverse intensity as a function of the square of the reduced wave vector $q\xi_0$ and (b) same data in a log-log plot.

dominated by the form factor of a thin film isotropically distributed in space (a two-dimensional object) and varies as $1/q^2$. Below $2\pi/\xi_0$ the scattering is dominated by thermal fluctuations of the membrane concentration. The shape of the scattering function describing this type of fluctuations is usually given by an Ornstein-Zernicke shape. However, due to the very special thermodynamics of the sponge, this is not the case [6, 11]. Indeed, due to the coupling of the symmetric/asymmetric order parameter and the concentration, the characteristic

scattering function is described by :

$$S(q) = 1 + B \frac{\text{Arctg } (q\xi_\eta/2)}{q\xi_\eta/2} \tag{1}$$

This unusual correlation function is the signature of the presence of the hidden order parameter η associated with the sponge symmetry [6, 11]. A more general formula includes direct density fluctuations with a correlation function ξ_ρ. In this case the scattering function becomes

$$S(q) = \frac{1}{1 + q^2 \xi_\rho^2} + \frac{B}{(1 + q^2 \xi_\rho^2)^2} \frac{\text{Arctg } (q\xi_\eta/2)}{q\xi_\eta/2} \tag{2}$$

When these fluctuations are negligible, the simplified form of the structure factor is recovered. In both cases, the deduced asymptotic behaviour of $S(q)$ which is reached at large q is qualitatively different from that obtained with an ornstein-Zernicke shape. When the η fluctuations are dominant $S(q)$ goes as $1/q$ at large q instead of the standard $1/q^2$ behaviour deduced from the Ornstein-Zernicke form.

The same analysis can be made in the asymmetric phase. The analog of (2) becomes [6] :

$$S(q) = \frac{1}{1 + q^2 \xi_\rho^2} + \frac{B}{(1 + q^2 \xi_\rho^2)^2} \frac{1}{1 + q^2 \xi_\eta^2} . \tag{3}$$

This means that the thermal fluctuations of the concentration come back to an Ornstein-Zernicke form when direct density fluctuations are negligible.

Since both ξ_0 and ξ_η can be arbitrarily large (of the order of several thousand ångströms), the form factor can also be in part accessible from light scattering. Since the Porod regime ($1/q^4$) is only seen with techniques using very small wavelengths and can never be observed with light scattering, we only need a description of the form factor of thin films to model this large q behaviour. We propose to use the following expression :

$$F(q) = \frac{A}{q^2 a^2} \left(1 - \exp(- q^2 a^2) \left(1 + \frac{q^2 a^2}{2} + \frac{q^4 a^4}{12} \right) \right) . \tag{4}$$

This function is similar to the form factor of disks at small q (the developments are similar up to q^4 terms). The same $1/q^2$ asymptotic behaviour is also obtained and is relevant in both the symmetric and asymmetric phases. The parameter a is directly proportional to the size of the sponge ξ_0. The plot of $q^2 F(q)$ as a function of q gives a plateau above the characteristic wave vector $q^* = 2/a$. Since q^* should be related to ξ_0 throught the relation $q^* = 2\pi/\xi_0$ we take the following :

$$\xi_0 = \pi a .$$

Note that the factor π deduced from the form factor of disks may be questioned. However in the next part we see that this expression gives an estimate of the sponge size in quantitative agreement with the values deduced from theory or extrapolated from neutron scattering. Moreover the discussion of the data relies on the variation of ξ_0 with ϕ rather than on its absolute value. Finally the complete expression of $I(q)$ used to fit the data either in the symmetric or the asymmetric side reads [12] :

$$I(q) = S(q) F(q) \tag{5}$$

where the general expression of $S(q)$ is (2) or (3) in the S and A phase, respectively.

This factorisation of $I(q)$ in terms of a structure and a form factor is only well established in special simple cases and may be questioned for a sponge phase. However this problem remains marginal in our case since most of the data are obtained when one of the two contributions is dominant.

Figure 2 gives a summary of the expected scattered intensity in the different regimes described above. Figure 2b presents a log-log plot while another way of presenting the same information ($1/I(q)$ as a function of q^2) is given in figure 2a to emphasize the large q regime. Both plots will be used in the next part to present the experimental results.

2.2 LIGHT SCATTERING RESULTS. — Results have been obtained along the dilution line previously labelled line B in reference [7] (see Fig. 1a). The results are essentially similar to that previously published. This new experiment was motivated by the importance of doing both light scattering and impedance measurements on the same samples, in order to discuss precisely the evolution of the samples with the membrane volume fraction. Typical results along this line are shown in figure 3. Samples are characterized by their membrane volume fraction calculated from the sum of the SDS plus the fraction of pentanol present in the membrane. A small amount of pentanol remains in the solvant. This fraction which is known to be close to 2 % corresponds to the solubility of pentanol in brine 20 g/l. As usual, the scattered intensity $I(q)$ of concentrated samples (like that shown in Fig. 3a) shows a typical figure with a downward curvature when $1/I(q)$ is plotted as a function of the square of the wave vector q. Approaching the S/A phase transition, S-shaped curves very close to a straight line are found (Figs. 2b and 2c). In reference [7], such curves were fitted using the complete form of the structure factor of the sponge (expression (2)) which incorporates the existence of direct density fluctuations. In this paper we propose another analysis to fit the data incorporating the form factor for the dilute samples ($\phi < 1$ %). Finally, in the A side, for the most dilute samples an upward curvature is found in the same plot (Fig. 3d). Such curves were previously analysed using expression (3) of the structure factor in the A phase where a linear coupling does exist between η and the membrane density.

The alternative analysis of the data is motivated by the fact that the characteristic distances of the sponge size below 1 % are larger than 3 000 Å. For sizes that large, it is necessary to consider the explicit form factor of the sponge (which is a form factor of a bilayer) to interpret the results. The scattered intensity previously normalized to the membrane volume fraction is plotted in figure 4 as a function of q in a log-log plot. Obviously the same asymptotic value is found at the largest wave vectors for dilute samples. A similar conclusion would be obtained from plots of $I(q) \cdot q^2$ as a function of q that show a plateau at large q. In figure 5 we give the dependence of this plateau with the membrane volume fraction which clearly shows a straight line. This characteristic behaviour is expected when the form factor of the sponge dominates and is commonly found with neutron scattering [10]. In the present case, we argue that the form factor should be considered for light scattering for samples with membrane volume fractions ϕ below typically 1 %. In fact, the corresponding sponge size $\xi_0 \approx 1.5\ \delta/\phi$ becomes of the order of 3 000 Å, i.e. of the order of the light wavelength ($\delta \approx 20$ Å is the membrane thickness deduced independently from neutron scattering). The optimum value of ϕ is obtained when the straight line extrapolates at the origin. This corresponds to a volume fraction of 2.1 % of pentanol present in the solvent. Note that with this remark we obtain an accurate calculation of the membrane volume fraction. If the alcohol concentration in water is different this will just slightly change the absolute value of the calculated volume fraction but will not change the conclusions.

Using the form of $I(q)$ introduced previously (Eq. (5)) gives satisfactory fits for the different samples along the dilution line. Fits are reported in figures 3 and 4 as continuous lines. As expected, the most concentrated samples are fitted with only the structure factor. In this case

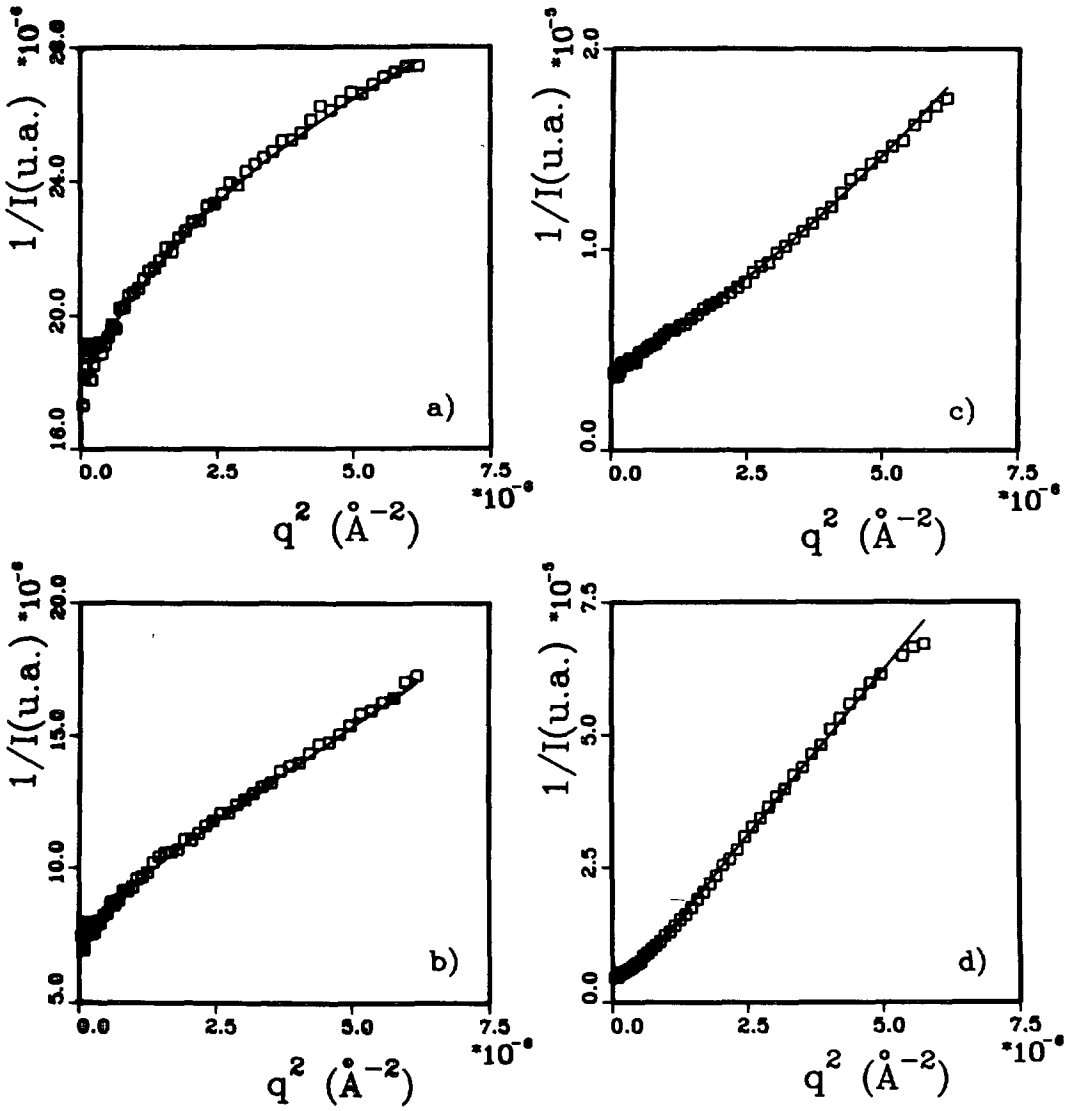

Fig. 3. — Typical light scattering results for samples with 20 g/l of NaCl, in a plot $1/I(q)$ as a function of q^2. The membrane concentrations are respectively : (a) $\phi = 2.63$ %, (b) 0.93 %, (c) 0.78 %, (d) 0.19 %. The continuous lines are the fits discussed in the text.

we can use the simplest expression of $S(q)$ (expression (1)). At higher dilution (typically when ϕ is between 0.8 and 1.3 %), the form factor (Eq. (4)) should be introduced while expression (1) is still used to describe the structure factor. Below $\phi \approx 0.8$ % the form factor alone can be used (we put $S(q) = 1$ in expression (5)), i.e. the structure factor becomes undetermined because of the very large values of ξ_η. As we see below, the S/A transition being located at $\phi \approx 0.3$ % it occurs when the form factor is dominant and only partial information on critical fluctuations can be obtained from these samples.

We now discuss the parameters deduced from the fit. When the structure factor is accessible from the experiment, we obtain $I(0)$, the extrapolated scattered intensity at $q = 0$ and the

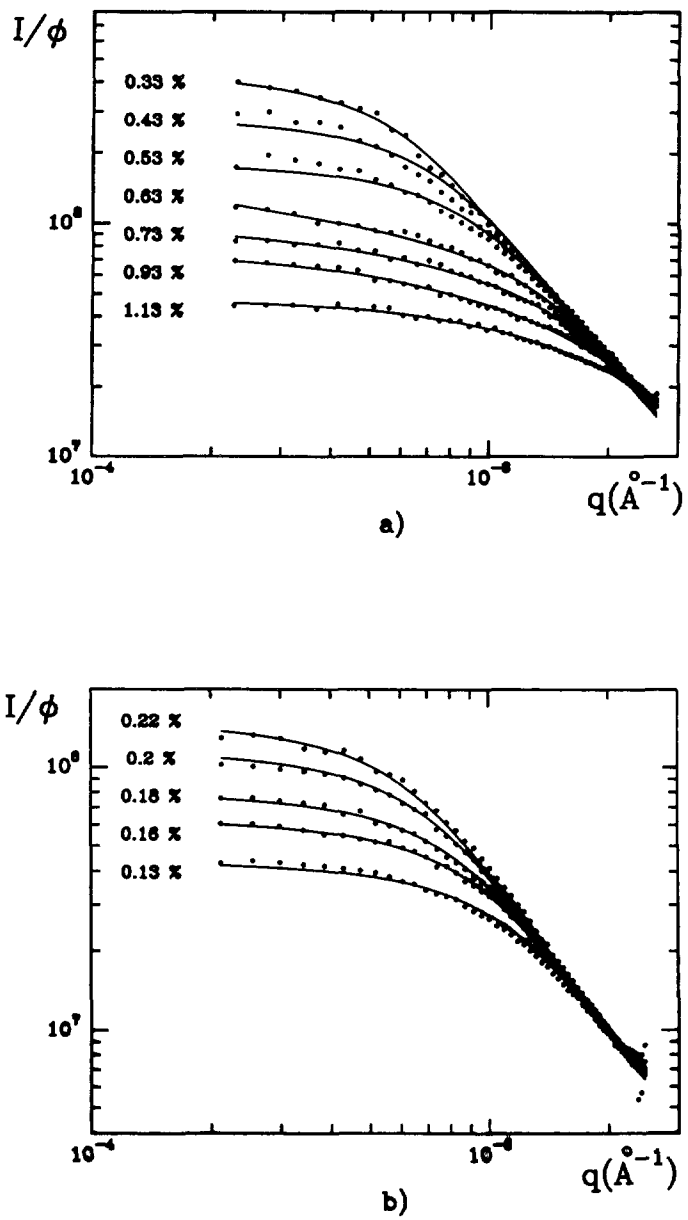

Fig. 4. — Similar data as in figure 3 in a log-log plot. The scattered intensity has been normalized to the membrane volume fraction. (a) Samples in the sponge domain, (b) samples in the asymmetric domain. The continuous lines are the fits discussed in the text.

correlation length ξ_η. Below 1.3 %, we also deduce the geometrical size of the sponge ξ_0 from the form factor. For the most diluted samples ($\phi < 0.8\,\%$) the structure factor becomes indeterminate. We still deduce ξ_0 and the parameter A (see expression (4)) which is the apparent extrapolated intensity at $q = 0$ (the real value of $I(0)$ being indeterminate).

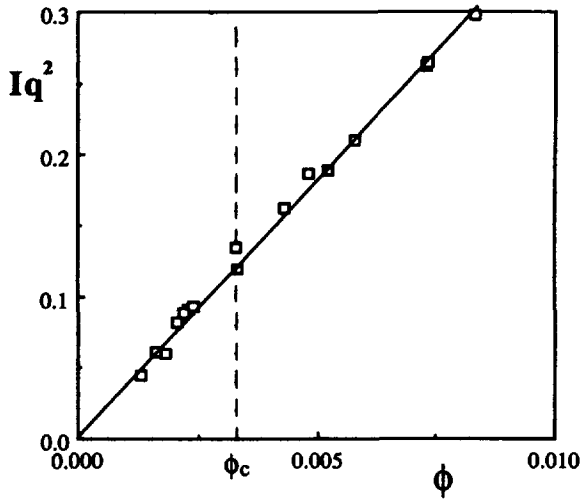

Fig. 5. — Plot of the large q (asymptotic) value of $I(q) \cdot q^2$ as a function of the membrane volume fraction. The location of the S/A phase transition is also given.

In figure 6 we give the variation of $1/\xi_0$ with the membrane volume fraction ϕ. For samples with $\phi > \phi_c = 0.3$ %, $1/\xi_0$ increases with ϕ, almost linearly as long as ϕ remains smaller than 1 %. This is the dependence expected for the (symmetric) sponge phase. The dotted and solid lines ((1) and (2) in Fig. 6) correspond respectively to the dependence predicted theoretically without ($d = \delta/\phi$) and with a renormalization (see equation below) of the elastic constant (with $\kappa = k_B T$) taking $\delta = 20$ Å as deduced previously from neutron scattering [13] :

$$d = \frac{\delta}{\phi}\left(1 + \frac{k_B T}{4\pi\kappa}\,\mathrm{Log}\,(\phi)\right).$$

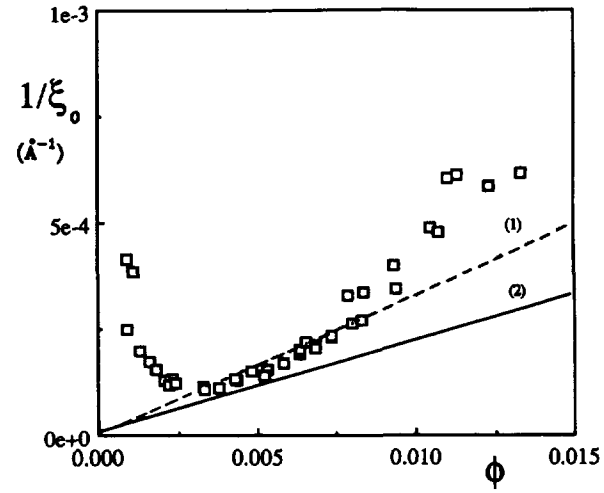

Fig. 6. — Plot of the inverse of the geometric length ξ_0 as a function of the membrane volume fraction. The dotted and solid lines (1) and (2) correspond to the dependence expected theoretically, without and with renormalisation of the elastic constant, respectively. The minimum of the curve gives the location of the S/A phase transition.

This shows the quantitative agreement with the present determination although we cannot discuss the relevance of renormalization effects. The less accurate data above 1 % should be considered more cautiously since for these samples the form factor remains marginal in the q dependence of the scattered intensity. The minimum of $1/\xi_0$ obtained at $\phi_c = 0.3$ % shows that the S/A phase transition should be located at this membrane concentration. This determination of the location of the S/A phase transition is therefore independent of any thermodynamic model but relies only on geometric arguments. Note finally that the rapid decrease of the characteristic size ξ_0 below ϕ_c is in agreement with the standard description of the asymmetric phase [6].

In figure 7 we give the intensity extrapolated at $q = 0$ ($I(0)$) obtained from the fit using Eq. (5). Note that for the samples which are the nearest from the A/S transition and if we take the accessible q-range into account ξ_η is so large that this value is probably underestimated. The results previously obtained [7] are also reported. As found previously, a maximum of $I(0)$ occurs at the phase transition. However it should be noted that in the vicinity of the maximum the form factor dominates the scattered intensity and this maximum is a consequence of the maximum of ξ_0 rather than the manifestation of a thermodynamic singularity. Supporting this analysis we give a log-log plot of the $I(0)\,\phi$ as a function of $\phi - \phi_c$ (inset of Fig. 7). The multiplication by ϕ is introduced to account for the dependence of the regular part of $I(0)$ which goes as $1/\phi$ when the logarithmic corrections are omitted. Compared with the result given in reference [7], there is a slight difference coming from a slightly different definition of ϕ. We had previously neglected the small amount of pentanol present in the solvent which is now taken into account to calculate ϕ. Following the present interpretation of the data, the singular behaviour associated with the phase transition should be visible when the structure factor is still present, i.e. above 0.8 %. $I(0)\,\phi$ presents two behaviours. For large values of $\phi - \phi_c$ the slope is quite large but for smaller values there is a clear crossover to a smaller exponent. Taking into account the way the $I(0)$ has been extracted and the fact that the exponent is sensitive to the precise definition of ϕ, it seems reasonable not

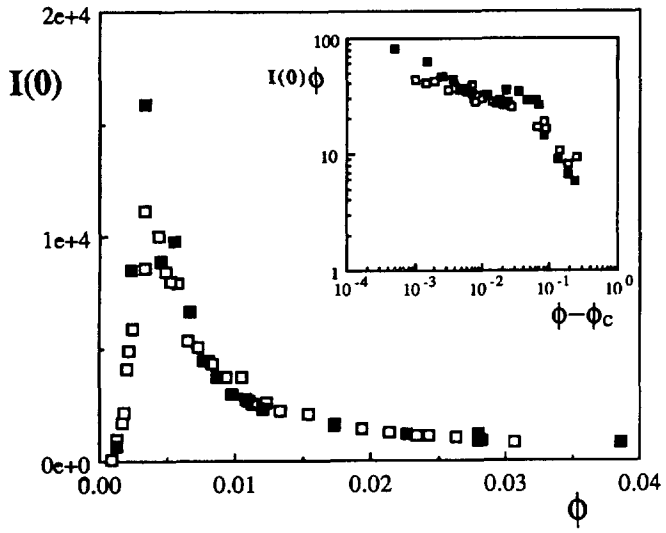

Fig. 7. — Light scattering intensity experimentally extrapolated at $q = 0$ along the dilution line : open squares, present results ; full squares, data of reference [7]. The variation of $I(0)\,\phi$ as a function of $(\phi - \phi_c)$ in a log-log plot is also given in inset.

to try to interpret the precise value of the exponents. The change in behaviour may be due either to a crossover from a strong divergence at large distance from the critical line to a weak divergence as expected from theory [6, 14] or to the fact that the compressibility of the phase is overestimated due to the limited q-range on which the data are fitted.

Figure 8 gives the variation of the correlation length ξ_η. We obtain a sharp increase when approaching the phase transition although no real critical behavior can be extracted from the data.

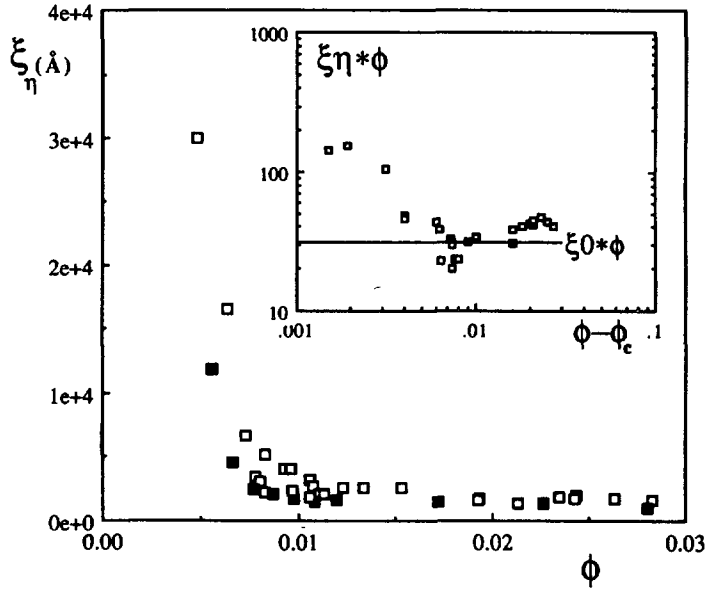

Fig. 8. — Variation of the correlation length ξ_η as a function of the membrane volume fraction open squares, present results ; full squares, data of reference [7].

In conclusion, we have shown that in order to fit the light scattering data of the most dilute samples it is necessary to take the bilayer form-factor into account. This allows us to determine the cell-size precisely as a function of the volume fraction and to characterize the Symmetric/Asymmetric transition precisely as a maximum of this cell-size. However, the limited q-range accessible with the experimental set-up and the very large values of the cell-size make the determination of the compressibility (as the inverse of $I(0)$) very difficult near the transition. Consequently a precise determination of a critical exponent approaching the second order line is difficult.

2.3 IMPEDANCE MEASUREMENTS. — We have also measured the impedance as a function of frequency in the range 100 Hz-15 MHz with a 4194 A Hewlett-Packard impedance analyzer. The sample is placed in a commercial Tacussel conductivity cell connected to the analyzer with a home-made connector. The impedance of the sample is readily obtained from the measurement after a compensation of the effect of the connections. This process requires three reference measurements, namely the empty cell, the cell filled with mercury to simulate a short-circuit and a « load » which should have an impedance close to that to be measured [15]. As the load, we took the solvent of the samples whose electrical characteristics are known in the frequency range of interest (as the impedance is independent of frequency). In particular,

this allows a correction of most of the polarisation effects which are always present in the two-probe geometry of the electrode. Since this correction is never perfect (the polarisation effects are not exactly the same for the solvent and a given sample), the data become unphysical at low frequency (usually below 10^3 Hz). After this compensation process, the complex conductivity $\sigma^*(\omega)$ of the sample is determined. A convenient way to present the data consists in giving the real part of the conductivity $\sigma(\omega)$ and the dielectric constant $\varepsilon(\omega)$. The data are presented as a function of the frequency ν ($\nu = \omega/2\pi$).

Typical results obtained along the dilution line are given in figure 9. The most concentrated samples have no frequency dependence of the impedance. For a smaller value of the volume fraction $\phi < 30\ \%$, a dielectric relaxation becomes visible as an increase of the conductivity and a decrease of the dielectric constant when the frequency is increased (Figs. 9a and b). This mode which has a characteristic frequency of the order of the MHz will be called « high frequency mode » in the following section. Approaching ϕ_C, a broader dielectric relaxation appears at a lower frequency (Figs. 9c and d). Note that for these samples the extrapolated dielectric constant at zero frequency becomes much larger (of the order of 10^5) than the corresponding value for the solvant (which remains close to 80). Note also that in this case, the high frequency mode is still present, superposed to the low frequency relaxation.

To analyse these results, one should consider that the present samples are composites made of a conducting solvent and a dielectric membrane. The free ions of the solvent contribute to

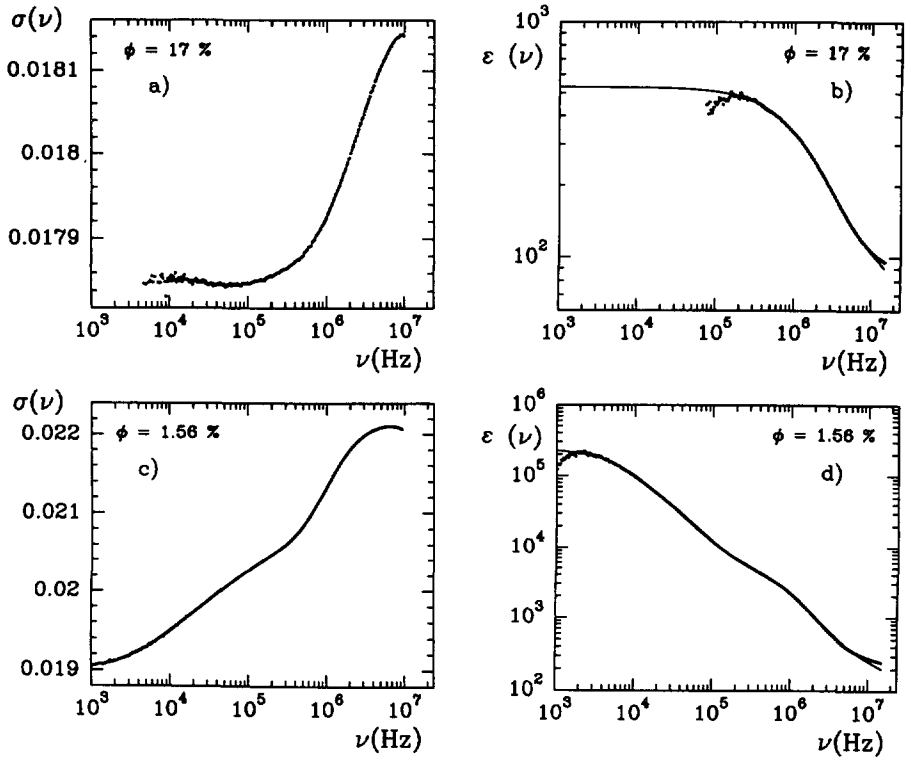

Fig. 9. — Typical results for the electrical conductivity $\sigma(\nu)$ ($\nu = \omega/2\pi$) and dielectric constant $\varepsilon(\nu)$: (a) and (b) for a concentrated sample ($\phi = 17\ \%$); (c) and (d) for a dilute sample ($\phi = 1.56\ \%$). The electrical conductivity is expressed in S/cm. The continuous lines are the fits discussed in the text.

the conductivity as the dielectric part of the signal comes from bounded charges. Therefore, we write the complex conductivity as a sum of a « free » and a « bounded » contribution.

$$\sigma^*(\omega) = \sigma_f^*(\omega) + \sigma_b^*(\omega) .$$

The former contribution being due to the free ions, we expect no frequency dependence in the present frequency range (typical ion relaxation times are of the order of 10^{-11} s) and identify $\sigma_f^*(\omega)$ with σ_{DC}. We attribute the frequency dependence of $\sigma^*(\omega)$ to the second contribution. Using the standard correspondence between σ and ε, we finally write :

$$\sigma^*(\omega) = \sigma_{DC} + i\omega\varepsilon^*(\omega)$$

with $\varepsilon^*(\omega) = \varepsilon(\omega) - i\varepsilon''(\omega)$. $\varepsilon(\omega)$ and $\varepsilon''(\omega)$ are not independent quantities since they are related through Kramers-Kronig relations [16]. As an example, we give in figure 10 the plot of $\varepsilon''(\omega)$ for the two samples chosen for figure 9.

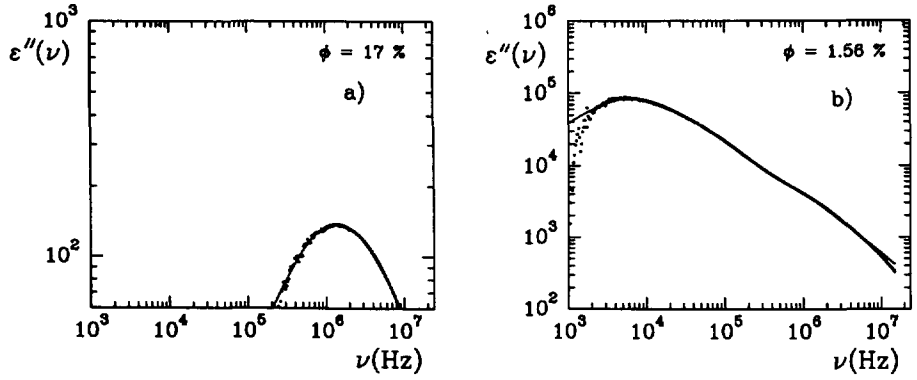

Fig. 10. — Imaginary part of the dielectric constant for the two samples of figure 9 : (a) ϕ = 17 %, (b) ϕ = 1.56 %. The continuous lines are the fits discussed in the text.

Examination of these two figures shows that the high frequency mode is close to a simple « Debye-like » relaxation. This is better illustrated by the corresponding « Cole-Cole » plot given in figure 11. Although the obtained figures are not semi-circles with a center on the ε axis, as expected for a real Debye relaxation, it should be noted that the figures remain symmetric and are in fact semi-circles with centers below the ε axis. Such a figure can be described by an empirical formula proposed by Cole and Cole [17], usually called the

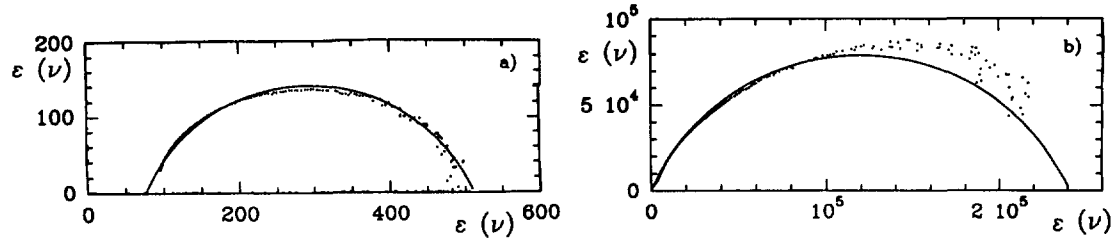

Fig. 11. — Cole-Cole plot of the samples chosen in figures 9 and 10 : (a) ϕ = 17 %, (b) ϕ = 1.56 %. The continuous lines are the fits discussed in the text.

« generalized » Debye formula

$$\varepsilon^*(\omega) = \frac{\Delta\varepsilon}{1 + (i\omega\tau)^{1-\alpha}} + \varepsilon_\infty$$

$\Delta\varepsilon$ and τ are respectively the intensity and characteristic time of the relaxation. The exponent α measures the departure from the simple Debye behavior which corresponds to $\alpha = 0$.

Figures 9, 10 and 11 show that good fits can be obtained by using this formula for both the high and low frequency modes. The general formula used to fit our data is therefore

$$\varepsilon^*(\omega) = \frac{\varepsilon_{hf}}{1 + i(\omega\tau_{hf})^{1-\alpha_{hf}}} + \frac{\varepsilon_{bf}}{1 + i(\omega\tau_{bf})^{1-\alpha_{bf}}} + \varepsilon_\infty$$

from which the real and imaginary parts of the dielectric constant are readily deduced. Finally, eight parameters : σ_{DC}, ε_{bf}, $\nu_{bf} = (2\pi\tau_{bf})^{-1}$, ε_{hf}, $\nu_{hf} = (2\pi\tau_{bf})^{-1}$, ε_∞, α_{bf} and α_{hf} are deduced from the fit and can be studied along the dilution line. Note that four of these parameters can be readily estimated from the experimental curves (σ_{DC}, ε_{bf}, ε_{hf}, ε_∞) and two others are not crucial for the fit (α_{bf} and α_{hf}).

From σ_{DC}, the obstruction factor is readily obtained by a normalization with the conductivity of an equivalent amount of solvent

$$S = \frac{\sigma_{DC}}{\sigma_{sol}(1 - \phi)}$$

where σ_{sol} is the conductivity of a solvent containing the same amount of ions as found in the sample, i.e. water salted with the same amount of NaCl plus SDS. Figure 12 gives the deduced obstruction factor. As already observed [10, 4], above 3 % a plateau is found with an obstruction factor close to 0.6. This plateau is the signature of the self similarity of the sponge, i.e. the invariance of the topology when adding solvent. The important result is the fact that S increases below $\phi^* \approx 3$ %, i.e. well before the phase transition at ϕ_C ($\phi_C \approx 0.3$ %) and therefore in the symmetric phase.

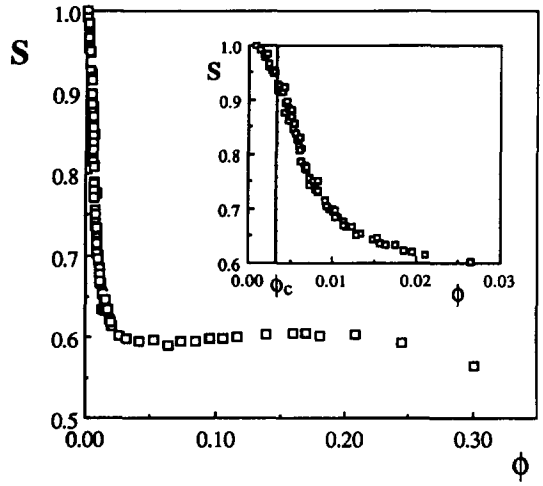

Fig. 12. — Obstruction factor for samples along the dilution line (20 g/l of NaCl). The dilute part of the curve is shown in inset.

Figures 13a and 13b give the variation of the intensity and characteristic frequency for the high frequency mode. Above ϕ^*, the intensity ε_{hf} of this mode goes like $1/\phi^2$ (solid line Fig. 13a). Below this concentration, we observe a departure from this simple law : a decrease of ε_{hf}. The characteristic frequency goes through a maximum at the S/A transition (at ϕ_c) as ε_{hf} almost vanishes. The simple behaviour observed above ϕ^* should again be considered as scaling laws. Therefore, this result confirms the departure from simple scaling laws in the symmetric phase, below ϕ^*

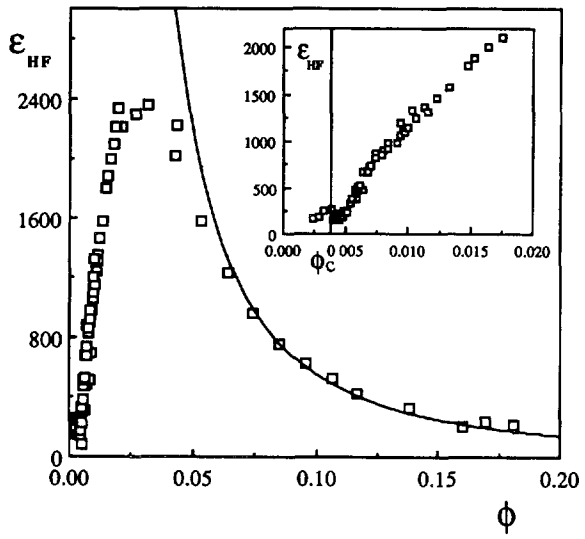

a)

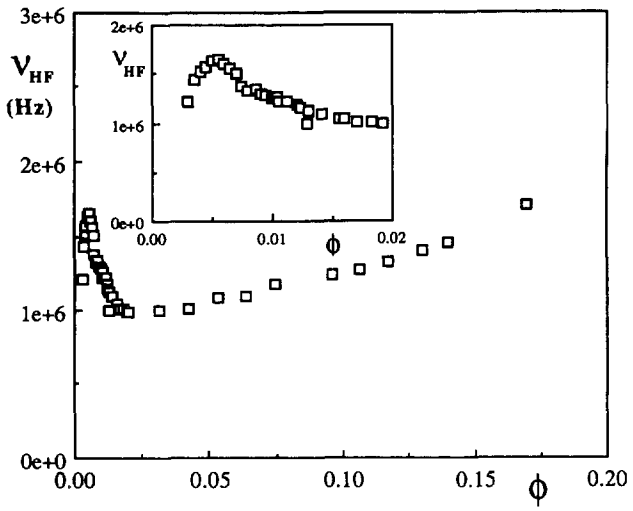

b)

Fig. 13. — (a) intensity of the high frequency mode (samples with 20 g/l of NaCl). The continuous line gives the scaling law ($\varepsilon_{hf} \sim 1/\phi^2$). The dilute part is given in inset where the location of the S/A phase transition is also given. (b) Corresponding characteristic frequency. A zoom for the dilute samples is given in inset.

Figures 14 give the variation of the intensity and characteristic frequency of the low frequency mode. This relaxation appears below ϕ^*. When ϕ decreases, its intensity increases quickly as ν_{bf} decreases. A maximum of ε_{bf} is observed around $\phi = 0.7$ % while a cusp is seen at the critical concentration ϕ_c. This mode quickly disappears in the asymmetric phase.

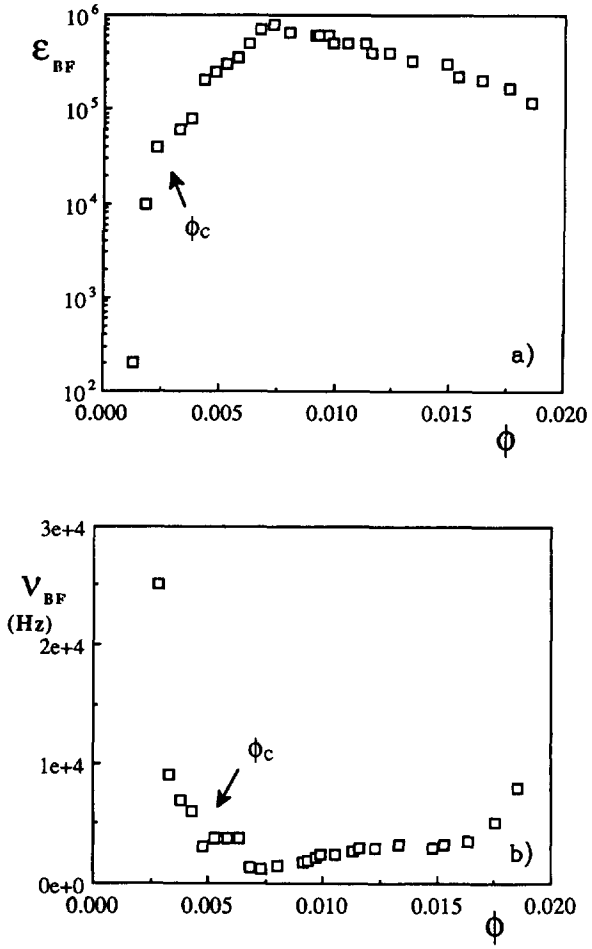

Fig. 14. — Intensity (a) and characteristic frequency (b) of the low frequency relaxation mode (samples with 20 g/l of NaCl) as a function of the membrane volume fraction. The location of the S/A phase transition is also given.

The results found for the exponents α_{hf} and α_{bf} as for ε_∞ will be presented in the next section since a better accuracy is obtained at a higher salt concentration.

Finally, we may summarize the main results as follows. At high concentration ($\phi > \phi^* \approx 3$ %) the obstruction factor deduced from the low frequency conductivity is constant and equal to 0.6. The high frequency mode is well described by a « generalized » Debye model with an amplitude $\varepsilon_{hf} \propto \phi^{-2}$ Below ϕ^* the system is still in a symmetric sponge phase (the characteristic length obtained from light scattering continues to increase as $1/\phi$) but several changes in the dielectric behaviour are noticeable.

i) The obstruction factor leaves the plateau and goes up.
ii) The intensity of the high frequency relaxation stops increasing and starts to decay.
iii) The characteristic frequency of this mode goes through a minimum.
iv) Another relaxation appears at lower frequency.

When the S/A transition is reached at ϕ_C, both the high and low frequency modes disappear very quickly.

3. Comparison with related systems with a higher concentration of NaCl.

We now compare the results obtained with 20 g/l with those corresponding to the samples with a higher salt concentration. We have studied dilution lines for a salt concentration of 30, 40, 50 and 80 g/l.

All these systems present similar phase diagrams. As an example, we give in figure 1b the phase diagram for 30 g/l. In each case, a dilution line was prepared to study the evolution of the physical properties with the membrane volume fraction. We successively compare in the following the light scattering and conductivity results.

3.1 LIGHT SCATTERING. — Very similar results are found when the salt concentration is increased. Far from the phase transition in the symmetric side, the structure factor showing an « Arctangent » dependence dominates as was previously mentioned. For more dilute samples, when ϕ becomes of the order of 1 %, the contribution of the form factor becomes significant. In figures 15 we give examples of the plots of $I(q)/\phi$ with a log-log scale. The biggest difference (compared with 20 g/l) is that the structure factor remains visible at small q around the S/A phase transition. However, the data at large q still give the asymptotic value of $I(q) \cdot q^2$ which varies linearly with ϕ (Fig. 16). Similarly the geometric size of the sponge can be deduced and is shown in figure 17. Therefore the critical concentration is readily determined. We obtain $\phi_C \approx 0.3$ %, which is approximately independent of the salt concentration.

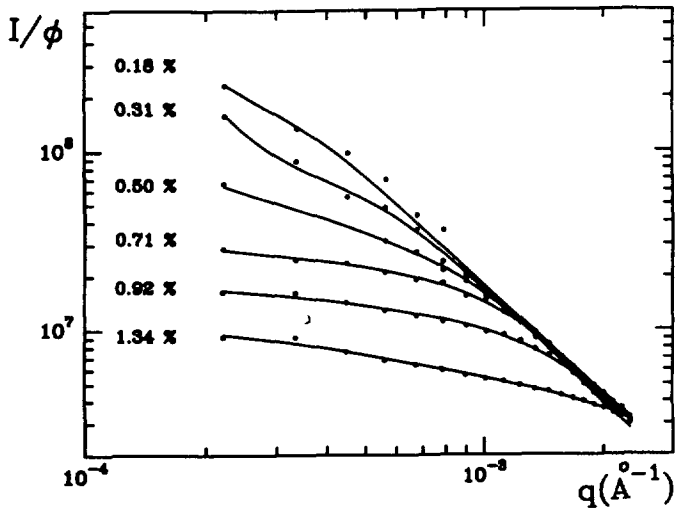

a)

Fig. 15. — Light scattering results along a dilution line. The normalized scattered intensity as a function of the wave vector in presented in a log-log scale. (a) System with 40 g/l of NaCl, (b) with 50 g/l of NaCl. The continuous lines give the fit discussed in the next.

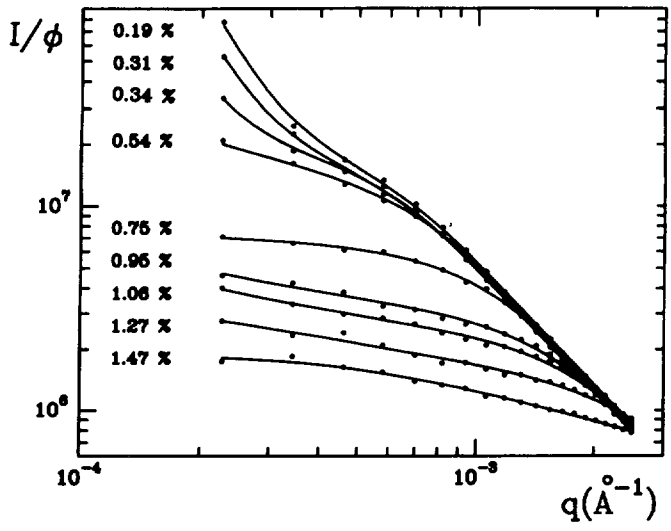

b)

Fig. 15 *(continued)*.

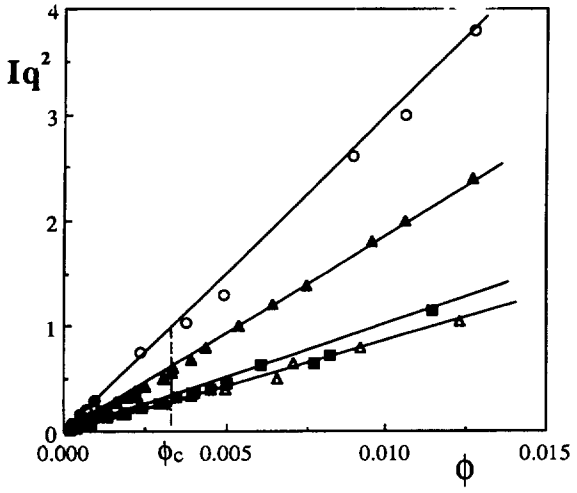

Fig. 16. — Plot of the large q (asymptotic) value of $I(q) \cdot q^2$: 30 f/l full squares, 40 g/l open triangles, 50 g/l full triangles and 80 g/l open dots.

The problem discussed for the concentration 20 g/l about the analyse of the structure factor is still in mind : because of the very large values of ξ_η reached near the phase transition, an accurate analysis of the structure factor would require a scattering experiment at smaller wave vector. However, the influence of $S(q)$ remains visible for values of ϕ below 1 % although it is clear that only asymptotic information corresponding to $q\xi_\eta > 1$ is accessible close to ϕ_c. In particular the real extrapolation of the scattered intensity at $q = 0$ remains indeterminate. As a consequence, a complete expression of the structure factor as (1) or (3) cannot be

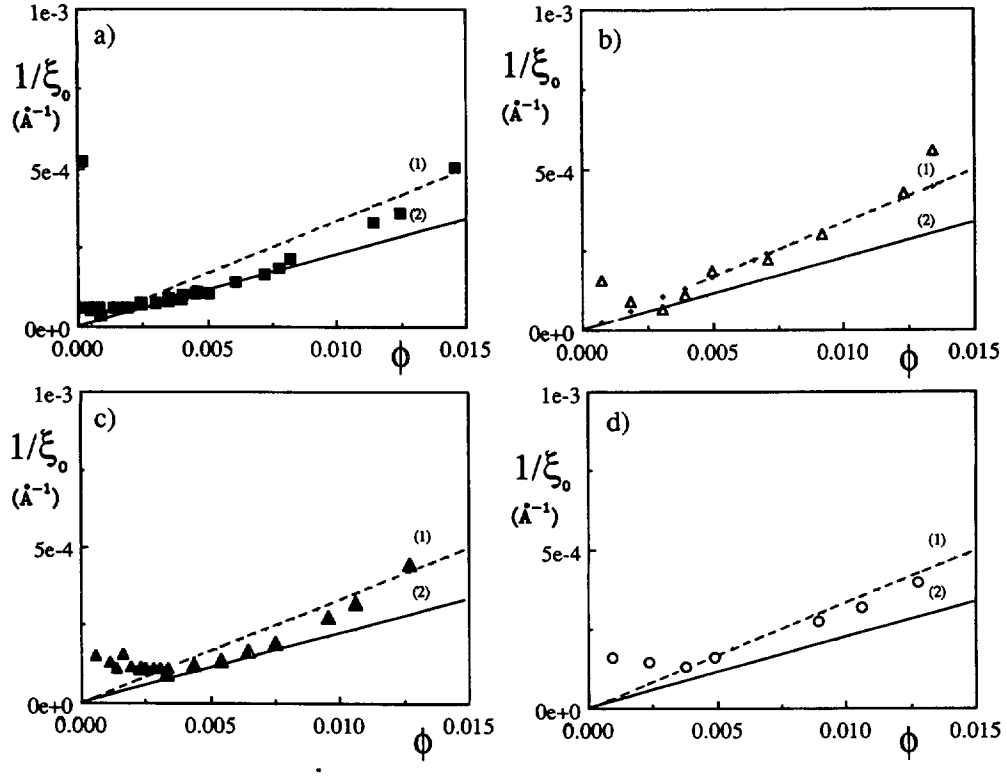

Fig. 17. — Plot of the inverse of the sponge size ξ_0 as a function of the membrane volume fraction : 30 g/l full squares, 40 g/l open triangles, 50 g/l full triangles and 80 g/l open dots. The dotted and solid lines (1) and (2) correspond to the dependence expected theoretically, without and with renormalisation of the elastic constant, respectively.

introduced to fit the data in the vicinity of the phase transition. Only the asymptotic expression deduced from these formulae should be considered, i.e.

$$S(q) \approx 1 + C\,(q)^{-x}$$

In the simple case where the η fluctuations are dominant, we expect $x = 1$ in the sponge phase but $x = 2$ in the A phase. Higher values of the exponent can be obtained if direct ρ fluctuations are also considered.

Experimentally, the best fits were obtained with $x = 1$ on the symmetric side, while a higher value of the exponent, $x \approx 4$ was found on the A side. It is remarkable that the distinct form of the structure factor in the two phases is still revealed by the asymptotic information obtained in the present experiment. In particular the value $x = 1$ found in the sponge phase should be considered as the signature of the « Arctangent » form of the structure factor.

3.2 ELECTRICAL MEASUREMENTS. — Let us now discuss the results obtained from the impedance measurements. As in the previous case, the conductivity and the dielectric constant were determined.

We first discuss the obstruction factor. A summary of the data is reported in figure 18. As the salt concentration increases, the volume fraction at which the obstruction factor leaves the plateau (ϕ^*) becomes smaller and smaller. The same information can be deduced from the

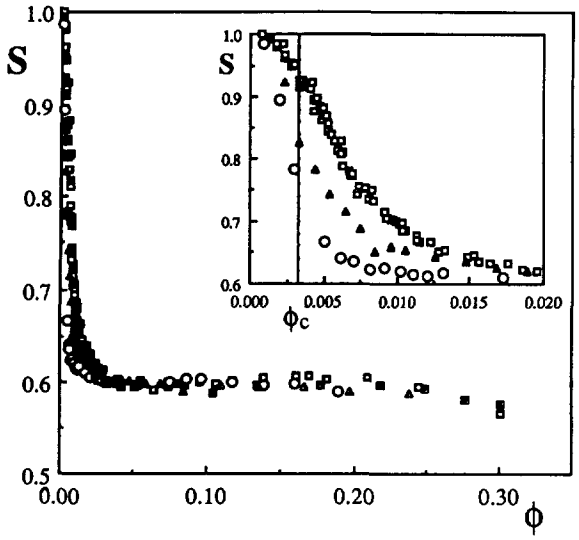

Fig. 18. — Obstruction factor along the dilution lines for samples with a different salt concentration. 20 g/l open squares, 30 g/l full squares, 40 g/l open triangles, 50 g/l full triangles and 80 g/l open dots. A zoom of the dilute part is given in inset for three salinities.

parameters of the high frequency mode. Figure 19 gives the intensity and the characteristic frequency of this mode. The departure from the simple scaling laws $\varepsilon_{hf} \sim 1/\phi^2$ and $\nu_{hf} \sim \phi$ occurs at lower and lower concentration as the salt concentration is increased. Since

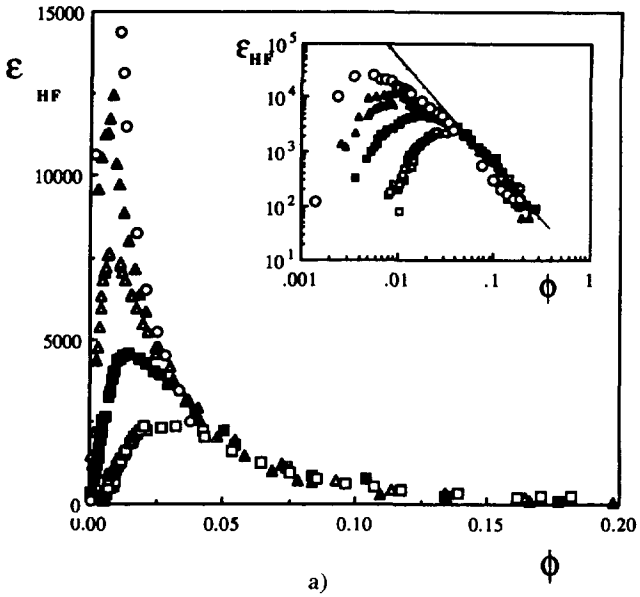

a)

Fig. 19. — (a) Intensity of the high frequency mode for samples with different salt concentrations as a function of the membrane volume fraction. The same data are given in inset with a log-log scale to emphasize the scaling law $\varepsilon_{hf} \sim 1/\phi^2$ obtained above ϕ^* (b) Characteristic frequency of these samples. Same symbols as before.

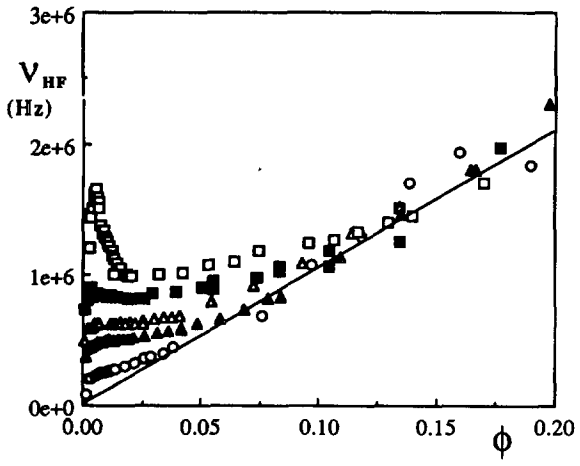

b)

Fig. 19 *(continued).*

the critical concentration ϕ_c is essentially constant this means that the difference $\phi^* - \phi_c$ decreases from 20 to 80 g/l.

Figure 20 gives the variations of the parameters for the low frequency mode for three different salt concentrations. As for 20 g/l, this mode appears below ϕ^*, at a frequency close to that of the high frequency mode. We give the intensity in figure 20a. For clarity only the data for three salt concentrations were reported. As the salt concentration increases, the maximum of the intensity becomes closer and closer to ϕ_c. The characteristic frequency, ν_{bf}, is still related to ε_{bf} as shown in figure 20b. We find an empirical relation $\varepsilon_{bf} \sim (\nu_{bf})^{-1.5}$ The fact that there exists a scaling law relating ε_{bf} and ν_{bf} (for the high frequency mode it is with an exponent 2 instead of 1.5) is the sign of a more general scaling either with the cell-size (for the

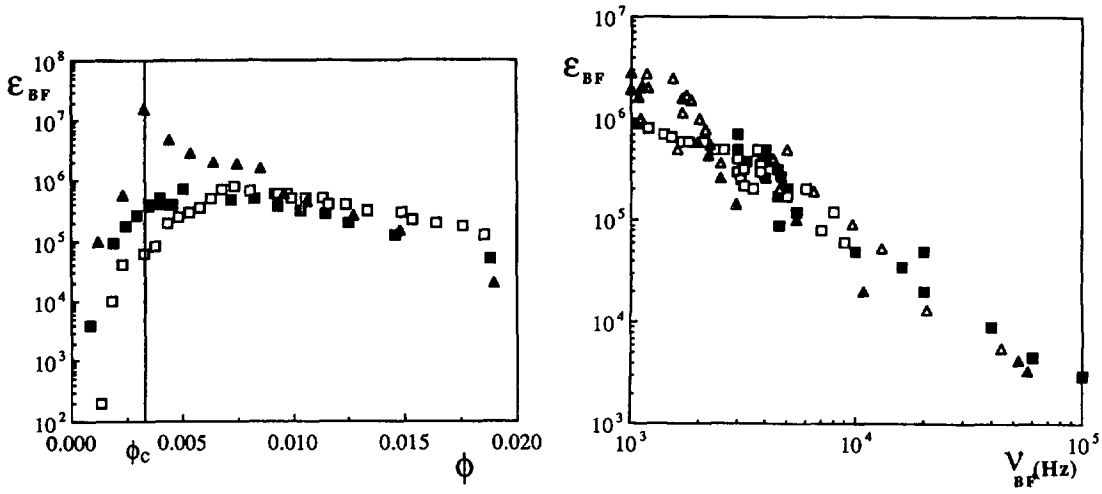

Fig. 20. — (a) intensity of the low frequency relaxation for samples with different salt concentrations as a function of the membrane volume fraction, (b) log-log plot of ε_{bf} as a function of ν_{bf} to show the relationship between these two parameters. Same symbols as before.

high-frequency mode) or approaching the second order transition line (for the low frequency mode). Note that the determination of the dielectric constant at low frequency becomes difficult at 80 g/l because of the high conductivity of these samples. However, it seems that the low frequency mode is much weaker in the latter case.

Figure 21 gives the results for the exponents α_{hf} and α_{bf}. Within the experimental error, a universal dependence (i.e. independent of the salt concentration) on ϕ is obtained in both cases. Both modes are closer to a Debye relaxation as the membrane concentration is decreased. This is particularly true for the high frequency mode which is very close to a simple Debye relaxation below $\phi = 1$ %.

Finally, in figure 22 we give the values obtained for ε_∞. Since ε_∞ is generally much higher than ε_{sol} this implies the existence of another relaxation above 15 MHz, ε_∞ being its intensity. It is clear that the shape of the obtained figure is qualitatively similar to that found for ε_{hf}. In particular a simple scaling law above ϕ^* with $\varepsilon_\infty \sim (\phi)^{-1}$ is evidenced by the log-log plot given in inset.

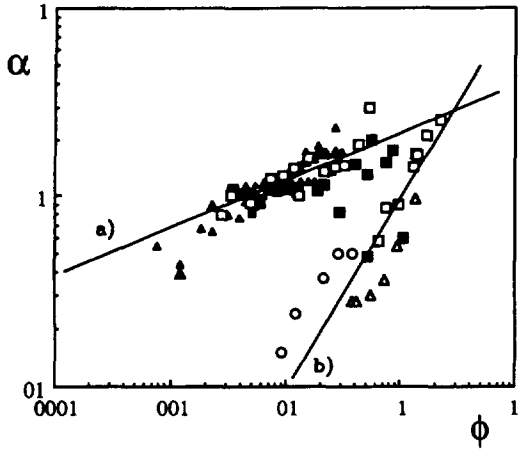

Fig. 21.

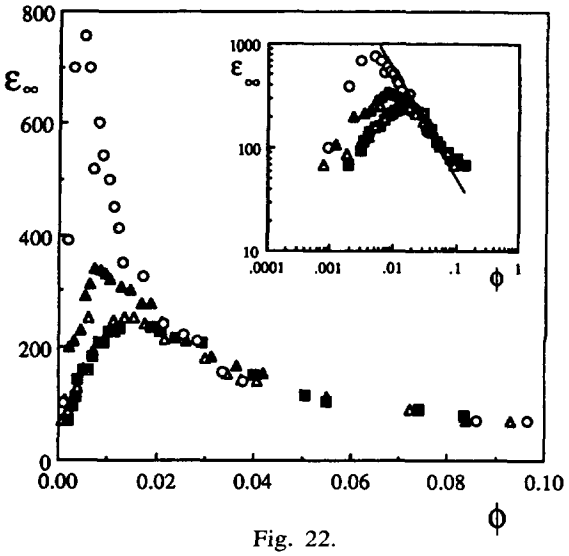

Fig. 22.

Fig. 21. — Variation of the low frequency exponent α_{bf}(a), and high frequency exponent α_{hf} (b) as a function of membrane volume fraction. Same symbols as before.

Fig. 22. — Plot of ε_∞ as a function of the membrane volume fraction for samples with different salt concentrations. Same symbols as before. The same data are given in inset with a log-log scale to emphasize the scaling law $\varepsilon_\infty \sim 1/\phi$ obtained above ϕ^*

4. Discussion.

The first point to mention is the new analysis of the light scattering data which allows a non-ambiguous determination of the critical concentration ϕ_c at the phase transition. Because of the very high dilution at which the S/A transition appears it is needed to take the form factor into account. However, most of the conclusions already found in reference [7] for the samples with 20 g/l of NaCl remain essentially unchanged. For example, the maximum of the scattered intensity is located at the second order phase transition. The plot of the geometric size ξ_0 of the sponge gives the ϕ dependence expected at a S/A phase transition, with in particular a

sharp decrease in the A phase. A similar analysis can be transposed to the samples with a higher salt concentration. The behaviour of ξ_0 remains essentially the same and ϕ_c is found to be approximately independent of the salt concentration. In all cases, the very large values of ξ_η prevent a complete analysis of the structure factor near the S/A phase transition. The consequence is that the exact determination of critical exponents close to the S/A line is made very difficult. Small angle light scattering is required in order to be able to measure the real compressibility in this range of dilution. However, the structure factor appears stronger for dilute samples as the salt concentration increases. This may suggest that a real tricritical behaviour is reached at the highest salt concentrations.

The new data concern the impedance measurements and in particular the determination of the dielectric constant. Once ϕ_C is determined from light scattering, this implies that all the data taken for $\phi > \phi_C$ concern the symmetric sponge phase. In fact, most of the electrical data concern the sponge phase. In particular, the crossover found at ϕ^* is in the sponge domain. The results can be classified into two groups.

The results above ϕ^* are representative of the sponge far from the S/A phase transition. In this region of the phase diagram, a plateau of the obstruction factor is found. At the same time, only the high frequency mode is present, with parameters which follow simple scaling laws, namely $\varepsilon_{hf} \sim 1/\phi^2$ and $\nu_{hf} \sim \phi$; As ϕ scales like $1/\xi_0$, this simply means $\varepsilon_{hf} \sim \xi_0^2$ and $\nu_{hf} \sim 1/\xi_0$. Therefore, it seems to be reasonable to relate this high frequency relaxation to the geometric size of the sponge. In the absence of any detailed dielectric model of the sponge phase, the only possibility is to compare this result with the dielectric behaviour of colloids, i.e. of dilute solutions of spherical dielectric objects of radius R in a conducting solvent. In this case, the simplest models lead to a Debye relaxation with an intensity proportional to R and a characteristic frequency proportional to $1/R^2$ [18, 19]. If ϕ is the volume fraction of spheres, the intensity of the relaxation is also proportional to ϕ. More sophisticated models give non-Debye relaxations but with still the same scaling for the intensity and characteristic frequency if the total charge of the particle remains the same [20, 21]. These results suggest that scaling laws may also be found in the sponge phase where ξ_0 plays the role of the characteristic size. However a simple transposition of the scaling laws deduced for spherical objects is impossible and more sophisticated modeling should be undertaken to explain the present results.

The results below ϕ^* should be discussed separately. In this case we observe an increase of the obstruction factor and a departure from the simple laws of the high frequency mode. At the same time, the low frequency relaxation appears. As we know from light scattering that we are still in the sponge phase above ϕ_C, with still the simple dilution law $\xi_0 \approx 1/\phi$, this behaviour should be associated with a subtle change of the structure of the sponge. The most natural explanation is the occurrence of holes in the membrane, i.e. a spontaneous generation of defects. In the absence of a model the dielectric constant, we shall essentially rely on the obstruction factor to discuss this point in more detail.

The data shown in figure 18 shows a strong influence of the salt concentration in the obstruction factor. There exist in fact two opposite interpretations for this result.

The simplest point of view is obtained starting from the ideal model of the sponge phase which neglects the presence of defects [2]. In this limit, the symmetry of the sponge is based on the fact that two sub-volumes of solvent separated by the membrane are equivalent and the obstruction factor is constant ($S_{pla} \approx 0.6$). Introducing defects (holes or spontaneous tearing of the membrane) suppresses the distinction between the two subvolumes. Therefore one may argue that the presence of defects breaks the sponge symmetry. Defects would then play the role of a small external field. This is equivalent to introducing a magnetic field for the paramagnetic-ferromagnetic phase transition. In this case, the signature will be a scaling

relation for the order parameter η and therefore for the obstruction factor S. Introducing H the conjugate field of η, we expect

$$\eta(\phi, H) = (\phi - \phi_c)^{\beta} f\left(\frac{H}{(\phi - \phi_c)^{\beta\delta}}\right).$$

Then, the departure from the plateau, $\Delta S = S - S_{pla}$ which is (at least for small values of η) proportional to η^2 reads

$$\Delta S \sim (\phi - \phi_c)^{2\beta} f^2\left(\frac{H}{(\phi - \phi_c)^{\beta\delta}}\right).$$

This scaling relation may be expressed by introducing $\Delta S_c \sim H^{2/\delta}$, the value of ΔS for $\phi = \phi_c$. We immediately deduce :

$$\frac{\Delta S}{\Delta S_c} = F\left(\frac{\Delta S_c}{(\phi - \phi_c)^{2\beta}}\right)$$

which can be used to analyse the data.

We may even propose an expression for the function F within the mean field approximation which should be appropriate close to a tricritical point. In this case $2\beta = 1$ and the equation of state for the order parameter is :

$$A'(\phi - \phi_c)\eta + \eta^3 = H$$

from which we deduce :

$$\frac{\Delta S}{\Delta S_c} = xy^2(x) \quad \text{with} \quad x = \frac{A'(\phi - \phi_c)}{H^{2/3}} \quad \text{and} \quad y + y^3 = x^{-3/2}$$

x being proportional to the « experimental » variable $(\phi - \phi_c)/\Delta S_c$.

The test for this scaling relation is given in figure 23a where we plot $\Delta S/\Delta S_c$ as a function of $(\phi - \phi_c)/\Delta S_c$. The continuous line is the mean field scaling function with $x = 166(\phi - \phi_c)/\Delta S_c$ in the domain $\phi > \phi_c$. The fact that a single curve is obtained in reduced units (which agrees with the theory) clearly supports this analysis.

There is however another interpretation following the point of view of Huse and Leibler [8]. In their study the sponge phase is not suppressed when defects are present. The departure from the plateau is then directly due to the presence of defects rather than being related to the vicinity of the critical point. In fact a single experimental curve given in figure 23b can be obtained by introducing a reduced membrane volume fraction ϕ/ϕ_0 where ϕ_0 is the volume fraction for which $S = 0.8$ (i.e. half way between the plateau and 1). ϕ_0 is roughly proportional to the volume fraction ϕ^* corresponding to the maximum of ε_{hf}.

From both interpretations, the nature of the phase transition is qualitatively the same whatever the salt concentration. In the first case, we are close to a second order S/A phase transition ideally reached for an infinite salt concentration. Within the second interpretation, the amount of defects is important to discuss the nature of the dilute phase (A or SFE). Since we do not see important deviation from « the ideal behaviour » with light scattering, so we expect that only a small number of defects are present in our systems and we suggest that we still observe a S/A phase transition. Then, this means that the obstruction factor is extremely sensitive to the presence of defects. We further discuss this point in the following.

The obstruction factor is proportional to the self-diffusion coefficient of the ions of the solvent in the presence of the membrane. This problem is related to the self diffusion of small

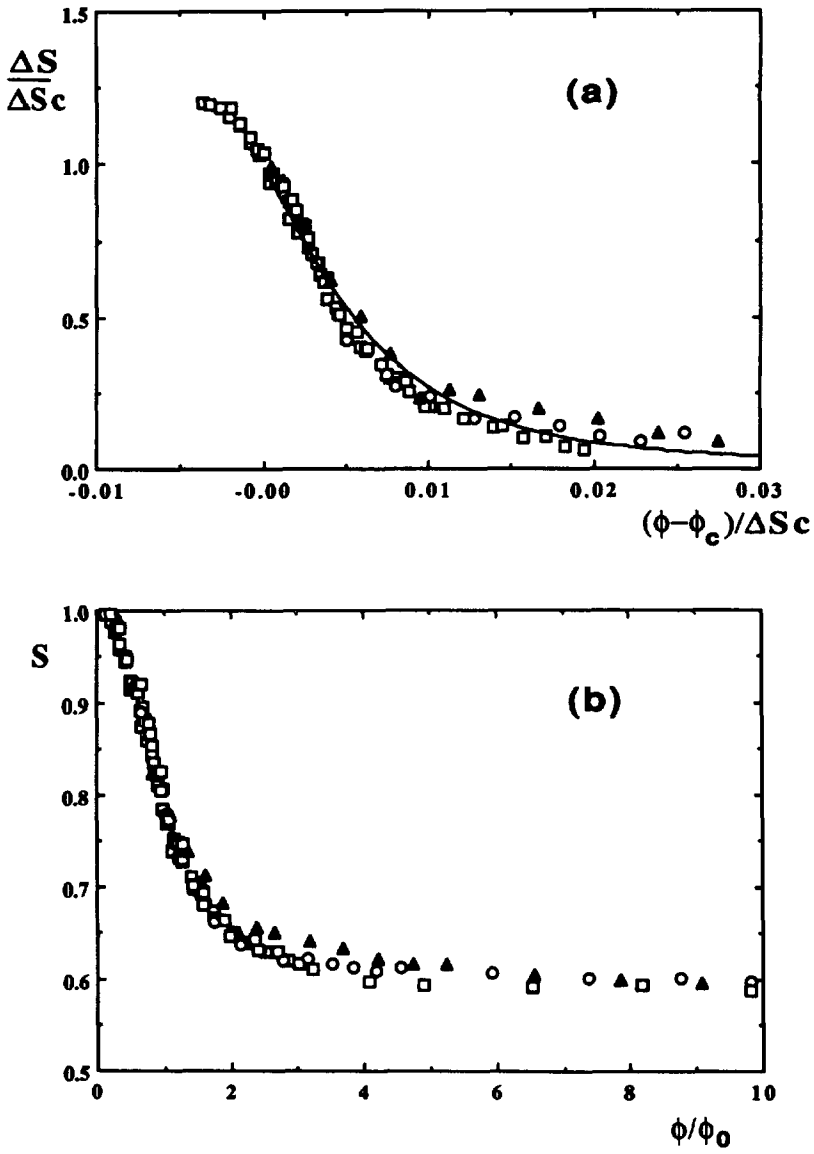

Fig. 23. — a) Reduced plot for the obstruction factor to show the possible scaling law. The continuous line gives the prediction of the mean field theory (see text). b) Plot for the obstruction factor using a reduced membrane volume fracton. Same symbols as before.

molecules in colloidal systems which has been discussed theoretically [22]. A cell model has been used to calculate the effect of varying the concentration of colloidal particles of different shapes. In particular, the obstruction factor has been calculated in the case of an oblate particle of various shape anisotopy R (R is the ratio between the short and long axes of the spheroidal particle). Typical results are reported in figure 24a. A limiting value of 2/3 is in fact obtained when $R = 0$ which corresponds to an infinite membrane. Therefore this calculation is relevant to estimate the obstruction factor of the sponge phase which is in fact close to 2/3 far from the S/A phase transition.

The same approach can be used to model the effect of defects on the membrane. Consider a spontaneous tearing of the membrane, L being the mean distance between two lines of edges. Instead of an infinite membrane ($R = 0$), we should now consider the obstruction by spheroidal objects of shape anisotropy $R = \delta/L$, the volume fraction of these objects being ϕ. The model described above gives the corresponding obstruction factor S. In figure 23b we give the variation of S as a function of R for two different values of ϕ in the dilute regime. It is clear that a very small value of R already gives a drastic increase of S above 0.66. Typically at $\phi = 1$ % the value $S = 0.9$ is reached as soon as R becomes of the order of 0.01, which means for $\delta = 20$ Å a mean distance between defect lines of the order of 2 000 Å. The same analysis with $S = 0.8$ leads to a mean distance between defects of the order of 5 000 Å.

Although this analysis is very simple, it certainly indicates that a very small number of defects can give a drastic effect on the obstruction factor and probably also on the dielectric constant. In particular, a mean distance between defect lines of the order or eventually larger than ξ_0 may be enough to explain the dielectric properties. This remark reconciles the light scattering and conductivity results. In fact, a proliferation of edges is not necessary to explain the conducting behaviour and the observed phase transition can still be close to a conventional S/A phase transition although defects are certainly present in the dilute part of the phase diagram. From our data the system with 80 g/l is that for which the presence of the defects is the most marginal, the important conclusion being that decreasing the salt concentration favors the presence of these defects. Samples with salt concentrations lower than 20 g/l may therefore show a more drastic effect of the defects and may eventually lead to a SFE phase. This point will be developed in paper II.

In addition to the high frequency relaxation, a low frequency relaxation is present close to the phase transition. This mode typically appears below ϕ^* and it is therefore tempting to try to relate its existence to the presence of defects. Supporting this argument, the low frequency relaxation remains marginal in the 80 g/l system. However, a complex behaviour of this mode is observed when changing the membrane volume fraction or the salt concentration as shown in figure 20. In particular, the maximum of the intensity occurs in the sponge domain at a membrane volume fraction which becomes closer to ϕ_c as the salt concentration increases. This maximum value goes above 10^6, i.e. at a value much larger than the dielectric constant of the solvent. The comparison with related systems with a lower salt concentration [9] suggests that the presence of the critical point in the dilute part of the phase diagram is essential to obtain such large values. If this statement is confirmed it means that the low frequency mode is in

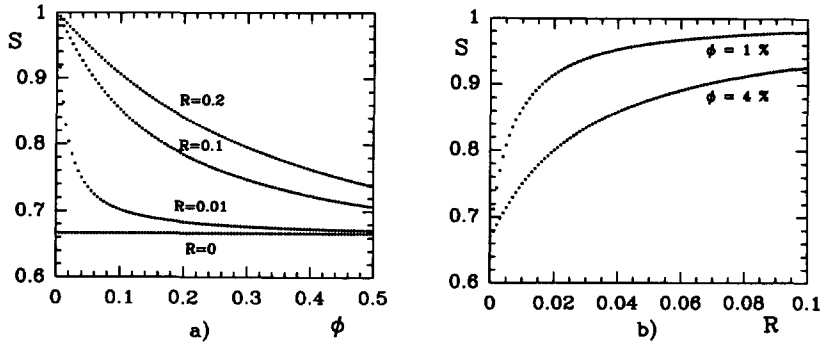

Fig. 24. — Obstruction factor calculated using the model of reference [21]. (a) Plot of S as a function of membrane volume fraction for different values of the shape anisotropy R. (b) Dependence of S as a function of R for two membrane volume fractions ($\phi = 1$ % and $\phi = 4$ %).

some way also related to critical fluctuations. In this case, the observed relation $\varepsilon_{bf} \sim (\nu_{bf})^{-1.5}$ would simply indicate that these two parameters are dependent on the same cut-off length (presumably the correlation length associated with the fluctuations) which should become very large as ε_{bf} becomes very large (and ν_{bf} becomes very small). The fact that the exponent α_{bf} remains positive when the high frequency mode is already very close to a Debye mode (see Fig. 21) may be associated with a « polydispersity » which is naturally present when observing critical fluctuations. In fact, the most natural explanation for a « generalized » Debye relaxation is the occurrence of a distribution of relaxation times [17]. In any case, the quantitative interpretation of the dielectric behaviour of the sponge phase near the S/A phase transition is certainly complex and is left for the future.

In conclusion, we have presented for the first time a study of the dielectric properties of a sponge phase near a second order S/A phase transition. The location of the phase transition was first obtained from a careful analysis of light scattering experiments. Then, the electric properties of the sponge (obstruction factor and dielectric constant) were described to show that defects on the membrane should be present in the vicinity of the phase transition although we think that the essential characteristics of the S/A phase transition are preserved. Moreover, the importance of the defects appears more and more important as the salt concentration is decreased from 80 to 20 g/l and the systems with a lower salt concentration are good candidates to study the role of these defects in more detail. This is the subject of a following paper.

Acknowledgments.

We thank J. P. Parneix for his advice when we started dielectric measurements. We thank A. Arneodo for suggesting the interpretation in terms of external field. We also thank M. E. Cates, F. Nallet and A. M. Bellocq for fruitful discussions and M. Maugey for technical help.

References

[1] Porte G., Marignan T., Bassereau P., May R., *J. Phys. France* **49** (1988) 511.
[2] Cates M. E., Roux D., Andelman D., Milner S. T., Safran S. A., *Europhys. Lett.* **5** (1988) 773.
[3] Gazeau D., Bellocq A. M., Roux D., Zemb T., *Europhys. Lett.* **9** (1989) 447.
[4] Strey R., Schomäcker R., Roux D., Nallet F., Olsson U., *J. Chem. Soc. Faraday Trans.* **86** (1990) 2253.
[5] Porte G., Appel J., Bassereau P., Marignan T., *J. Phys. France* **50** (1989) 1335.
[6] Roux D., Coulon C., Cates M. E., *J. Phys. Chem.* **96** (1992) 4174.
[7] Coulon C., Roux D., Bellocq A. M., *Phys. Rev. Lett.* **66** (1991) 1709.
[8] Huse D. A., Leibler S., *Phys. Rev. Lett.* (1991) 437.
[9] Coulon C., Bellocq A. M., Nallet F., Roux D., Alibert I., Vinches C. (to be published).
[10] Gazeau D., PhD thesis, Bordeaux (1989).
[11] Roux D., Cates M. E., Olsson U., Ball R. C., Nallet F., Bellocq A. M., *Europhys. Lett.* **11** (1990) 229.
[12] Since the sponge should be modeled as a complex deformable object, a simple factorisation between the two contributions is however not obvious.
[13] Roux D., Nallet F., Freyssingeas E., Porte G., Bassereau P., Skouri M., Marignan J., *Europhys. Lett.* **17** (1992) 575.
[14] Coulon C., Roux D., Cates M. E., *Phys. Rev. Lett.* **67** (1991) 3194.

[15] Vinches C., PhD thesis, Bordeaux (1994).
[16] Kramers H. A., *Atti. Congr. Int. Fysici, Como* **2** (1927) 545 ;
Kronig R., *J. Opt. Soc. Am.* **12** (1926) 547.
[17] Cole K. S., Cole R. H., *J. Chem. Phys.* **9** (1941) 341.
[18] Schwarz G. J., *J. Chem. Phys.* **66** (1962) 2636.
[19] Schwan H. P., Schwarz G., Maczuk J., Pauly H., *J. Phys. Chem.* **66** (1962) 2626.
[20] Fixman M., *J. Chem. Phys.* **78** (1983) 1483.
[21] Chew W. C., Sen P. N., *J. Chem. Phys.* **77** (1982) 4683.
[22] Jonsson B., Wennerstrom H., Nilsson P. G., Linse P., *Colloid Polymer Sci.* **264** (1986) 77.